



UNIVERSITY OF LEEDS

This is a repository copy of *Nano-scale coating wear measurement by introducing Raman-sensing underlayer*.

White Rose Research Online URL for this paper:
<https://eprints.whiterose.ac.uk/173042/>

Version: Accepted Version

Article:

Xu, N orcid.org/0000-0002-8291-6519, Wang, C orcid.org/0000-0002-4301-3974, Yang, L orcid.org/0000-0003-0935-3921 et al. (4 more authors) (2022) Nano-scale coating wear measurement by introducing Raman-sensing underlayer. *Journal of Materials Science and Technology*, 96. pp. 285-294. ISSN 1005-0302

<https://doi.org/10.1016/j.jmst.2021.04.031>

© 2021 Published by Elsevier Ltd on behalf of Chinese Society for Metals. This manuscript version is made available under the CC-BY-NC-ND 4.0 license
<http://creativecommons.org/licenses/by-nc-nd/4.0/>.

Reuse

This article is distributed under the terms of the Creative Commons Attribution-NonCommercial-NoDerivs (CC BY-NC-ND) licence. This licence only allows you to download this work and share it with others as long as you credit the authors, but you can't change the article in any way or use it commercially. More information and the full terms of the licence here: <https://creativecommons.org/licenses/>

Takedown

If you consider content in White Rose Research Online to be in breach of UK law, please notify us by emailing eprints@whiterose.ac.uk including the URL of the record and the reason for the withdrawal request.



eprints@whiterose.ac.uk
<https://eprints.whiterose.ac.uk/>

Nano-scale coating wear measurement by introducing Raman-sensing underlayer

Nan Xu,^{1,*} Chun Wang,¹ Liuquan Yang,¹ Eric Kumi Barimah,² Gin Jose,² Anne Neville,¹ and Ardian Morina¹

¹ *Institute of Functional Surfaces, School of Mechanical Engineering, University of Leeds, Leeds LS2 9JT, United Kingdom*

² *School of Chemical and Process Engineering, University of Leeds, Leeds LS2 9JT, United Kingdom*

*Corresponding author: mnnx@leeds.ac.uk (Nan Xu).

Abstract

For gaining fundamental insights into coating wear mechanisms and increasing operational efficiency and automation degree of equipment in important application fields of coating techniques, it is of great importance to develop novel wear measurement techniques enabling nanoscale studies of coating wear in the running process, but this still remains a significant challenge. Here, a facile strategy is reported to achieve accurate coating thickness quantification at nanoscale level, which is based on a bilayer structure: a top target layer of a-C:H (hydrogenated amorphous carbon) film is considered as a light attenuating and anti-wear layer while underlayer of silicon serves as Raman-sensing layer. Through constructing the relationship between thickness of a-C:H and Raman intensity of attenuated silicon signal, coating thickness quantification method is established and successfully applied to quantify coating wear in the friction process. This approach can effectively avoid remarkable errors caused by tribo-induced effects in the interface regions, demonstrating its advantage in error tolerance. Details about these tribo-induced effects are also elucidated by combination of Raman spectroscopy, optical profilometer, EELS, and TEM. In particular, the proposed approach enables the possibility of measuring coating wear with oil film on top, which breaks an important limitation of

existed wear measurement methods, i.e., incapable of applying in oil-lubricated conditions. This approach can be used to quantify the wear condition of diverse target coatings and has the potential of online wear monitoring when combining a compact laser excitation and detection system.

Keywords: Coating; Wear measurement; Raman; Layered structure; Nanoscale

1. Introduction

Over recent decades, coating technique has been widely used in diverse engineering fields such as manufacturing, automobiles, aeronautics, micro-electromechanical systems, biomedical devices, etc [1-3]. In these applications, wear of coating, particularly on the key components, critically affects the service life and reliability of systems/devices. For gaining key and necessary information of wear condition and failure prediction, it is therefore necessary to develop accurate and reliable coating wear measurement techniques, particularly at nanoscale level. In fact, coating failures on moving parts generally origin from surface micro-damage, like micro-pitting or micro-crack. Nanoscale studies of wear can provide valuable and fundamental insight into wear mechanisms of coatings, which are crucial for extending the lifetime and durability, increasing the operational efficiency, as well as decreasing energy consumption. Meanwhile, since modern industry in the era of Industry 4.0 strives to drive machines to cooperate in more robust and autonomous way with minimum downtime, maintenance strategies are transforming from traditional reactive practices to predictive and preventive methodologies [4,5]. Given the growing demand of automation, online monitoring capability is also strongly required for wear measurement techniques.

Up to now, most approaches of online wear monitoring estimate wear conditions based on the multi-sensor signals which are indirectly correlated to wear, such as acoustic emission, cutting force, vibration and motor power [5-9]. Their inherent drawbacks, deriving from signal noise and lack of direct or visual wear information, always lead to

inevitable reduction in measurement reliability and accuracy [6,7]. In addition, since these methods are incapable of direct application in a distinct service condition, model retraining become necessary, which requires extensive tests to obtain various operation parameters for estimating wear level [8,9]. In comparison, highly reliable and accurate topographic analysis of surface wear can be achieved via direct wear measurement approaches in the form of two- or three-dimensional wear profiles. Currently, there are two typical modes of direct approaches widely used in industrial fields: stylus and non-contact optical profilometer [10,11]. The significant advantage of former approach is that it captures real physical depth profile by using touch trigger probes. However, it cannot provide continuous online measurements because the contact regions of moving parts are generally inaccessible during running process. The non-contact optical approach builds up three-dimensional topographic map by collecting array signals of light interference of reflected light. Although highly accurate surface analysis at nanoscale can be achieved for as-grown coatings via non-contact optical approach, remarkable measurement errors will appear when characterizing the tribo-tested coatings as indicated in this study. Since non-contact optical approach possesses high sensitivity on the light signals, tribo-induced variation of optical properties on the coating surface, which can be termed as tribo-induced polishing effect [12], can significantly affect reflected light signal, further leading to remarkable measurement errors.

Consequently, there is a request to develop novel coating wear measurement approaches that can provide accurate wear information at the nanoscale while possessing online monitoring and high error tolerance capabilities and enabling directly implementation in various engineering fields. With the development of highly compact laser excitation and detection system expected in near future, coatings with built-in wear sensing layer may open a new pathway for fulfilling the request. As reported in the previous studies [13,14], through embedding discrete sensor layers with Raman signals

inside the tribological coating, a multilayer coating system with wear sensing capability was constructed. By monitoring the Raman signal during the friction process, this system could report the wear depth and failure warning. However, the relationship between the Raman signal intensity of sensor layer (sublayer) and the thickness of upper layer remained unexplored. Several studies by Scharf *et al.* proposed a Raman scattering model for quantifying the thickness of Raman active coating (i.e., diamond-like nanocomposite (DLN)) [15,16]. By clarifying the correlation between DLN thickness and the Raman intensity of carbon signal of DLN in the form of equations, this model allowed us to provide more detailed wear information in the form of wear depth profile. However, the influence of tribo-induced effects on measurement accuracy was not considered in these studies, which could lead to remarkable measurement errors, especially for the long term tribological tests. As indicated in our study, since Raman spectra of carbon signal of DLN are dominated by scattering of sp^2 phase due to its high polarizability, even slightly tribo-induced enhancement of sp^2 phase could result in remarkable increase of carbon signal intensity [17], further leading to obvious measurement errors in the bonding transformation regions. We noted that the challenges posed by the long-term operation included exploring the mechanisms of tribo-induced effects and minimizing their influence on measurement errors for lifting the error tolerance capability.

Inspired by the coating systems with built-in wear sensing layer, a facile and accurate coating thickness measurement approach was developed by employing a bilayer structure with the top target layer of a-C:H as light attenuating and anti-wear layer and bottom layer of silicon as Raman-sensing layer. Here, the main reason of selecting a-C:H as target coating is that such coatings have already been applied in many industrial applications. Through establishing the relationship between the thickness of as-grown a-C:H films and Raman intensity of silicon signal, a coating thickness quantification method was constructed, which was further employed to measure the coating wear in both dry and oil-

lubricated conditions. Compared with other wear measurement methods, e.g., optical profilometer and the method proposed by Scharf *et al.*, this approach provided more accurate and detailed wear information in the form of wear profile, avoiding the remarkable errors arising from the tribo-induced polishing effect and bonding transformation in the interface regions, especially in the long term tribological tests. Details about these tribo-induced effects were also elucidated by combination of Raman spectroscopy, optical profilometer, electron energy loss spectroscopy (EELS), and transmission electron microscopy (TEM). While this paper is more focused on development and verification of the coating wear quantification method by theoretical and experimental experiments, future studies will transfer the coating systems (top target coating/Raman sensing underlayer) on the surface of workpieces and focus on optimizing the online wear monitoring capability by combining a compact laser excitation and detection system.

2. Experimental Section

2.1. Synthesis of hydrogenated amorphous carbon films (a-C:H)

The a-C:H films were deposited by a Plasma Enhanced Chemical Vapour Deposition technique (PECVD) with acetylene as gas precursor (Flexicoat 850, Hauzer Corp., Netherlands). Two kinds of substrates, n-type silicon (100) wafers (10 mm × 10 mm × 0.5 mm, Ra < 1 nm) and glass plates (25 mm × 25 mm × 1 mm, Ra < 1 nm), were employed. The a-C:H films deposited on silicon wafers were used for tribo-test, thickness quantification, and characterizations of structure and composition, while those on glass plates were for optical studies. More details of film deposition procedure can be found in the supplementary material. The deposition time of the a-C:H films with thickness of ~15, 37, 110, 183, and 277 nm was 15 mins, 30 mins, 50 mins, 100 mins, and 130 mins, respectively. Additionally, silicon wafer was partially marked for measuring the thickness of a-C:H films by NPFLEX 3D non-contact optical profilometer as shown in Figure S1.

2.2. Tribological Experiments

The tribological experiments were conducted via a UMT ball-on-disc tribometer at room temperature under both dry and oil-lubricated conditions. The samples with a-C:H films deposited on silicon wafers were clamped on a reciprocating platform, using a fixed upper ball (AISI 52100 steel, 6.35 mm in diameter, HRC 60-67) as the counterpart. In oil-lubricated conditions, pure PAO4 base oil was employed as lubricant.

2.3. Materials Characterization

Raman spectroscopy (inVia Renishaw system) was used to quantify the thickness of a-C:H films in a line-scanning mode with 488 nm laser and 180° backscattering geometry. Raman spectra were obtained with 1 mW laser power. By employing 50× objective lens, the lateral resolution could reach 1 μm. As indicated in section 2.1, the silicon wafers were etched in argon plasma before depositing a-C:H. Considering the effect of etching process to the Raman signal of silicon wafer, a standard silicon wafer was etched in the same condition and tested first to obtain the Raman intensity of silicon without attenuation ($I_0\beta$) before every Raman line-scanning test of a-C:H films, as displayed in Figure 1a. NPFLEX 3D non-contact optical profilometer and TALYSURF 120L contact profilometer were employed to characterize the wear scars and verify the quantified results based on Raman spectroscopy. UV-vis-NIR spectroscopy (PerkinElmer Lambda 950) was employed to study the optical properties of a-C:H films deposited on glass plates.

A focused ion beam (FIB, FEI Helios G4 CX DualBeam FIB-SEM) was used to prepare thin cross-sectional lamellar specimens of friction contact area for the characterizations of transmission electron microscopy (TEM) and electron energy loss spectroscopy (EELS). Prior to FIB milling, the contact area was coated by a layer of iridium (20 nm) to eliminate contaminations. Then, samples were transferred into FIB-SEM chamber and coated by a thick Pt film (~ 1 μm) in order to protect coating structure during FIB milling (low-kV Ga⁺ ion milling). FEI Titan3 Themis 300 TEM/STEM (Scanning transmission

electron microscopy) equipped with Gatan Quantum ER energy filter was employed for TEM and EELS characterization. Note that EELS in STEM mode could provide detailed information of bonding structure in the atomic resolution [18, 19]. EELS spectra of C-K core-edge were collected point by point across the specimens. Gaussian peak fitting was adopted to quantify the bonding fractions and more details are presented in S1 (section S1.2).

3. Results and discussion

3.1. Construction of Coating Thickness Quantification Method

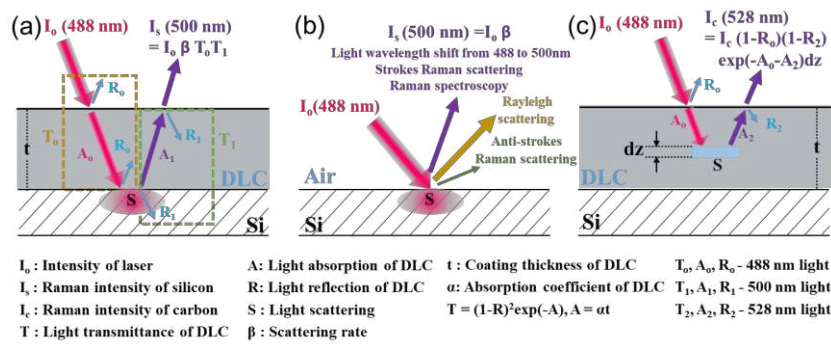


Figure 1. Schematic illustration of coating thickness quantification methods under dry friction. (a) Coating thickness quantification method based on the Raman signal of silicon substrate. (b) Light wavelength shift on the sites of Raman scattering. (c) Coating thickness quantification method based on the Raman signal of carbon films.

A schematic of the proposed wear quantification method in this study is shown in Figure 1a. In our method, Si wafers served as Raman signal provider due to its high intensity of silicon 1st band at 520 cm^{-1} and a-C:H coatings were deposited on top and employed as anti-wear and light attenuating layer. Since light intensity will be attenuated in a-C:H due to absorption (A) and reflection (R), the Raman intensity of silicon signal (I_s) of silicon substrate depends on the transmittance values of both incident light (I_o) and scattered light and is given based on Beer's law by

$$I_s = I_o \beta T_o T_1 \quad (1)$$

where β is light scattering rate, $I_o \beta$ is Raman intensity of silicon 1st band of silicon substrate (Figure 1b), and T_o and T_1 are transmittance values of incident light and scattered light respectively. Additionally, it should be pointed out that there exists shift of light

wavelength on the sites of Raman scattering. As shown in Figure 1a,b, when employing silicon substrate as Raman signal provider, the wavelength (λ_o , 488 nm) of incident light will shift to 500 nm (λ_1 , scattered light), according to the equation [20]:

$$\lambda_1 = \frac{1}{\frac{1}{\lambda_o} - \nu} \quad (2)$$

where ν is Raman shift (520 cm^{-1} for silicon 1st band).

By substituting the transmittance (T) in the equation (1) with the following expression [21]:

$$T = (1 - R)^2 \exp(-A) = (1 - R)^2 \exp(-\alpha t) \quad (3)$$

where α is the light absorption coefficient and t is the thickness of a-C:H coating (unit: μm), the relationship between I_s and t can be constructed by:

$$I_s = I_o \beta (1 - R_o)^2 (1 - R_1)^2 \exp(-\alpha_o - \alpha_1) t \quad (4)$$

where R_o and α_o are the reflectivity and absorption coefficient of a-C:H for incident light (488 nm), and R_1 and α_1 are that for scattered light (500 nm). The thickness of a-C:H can be obtained through rearranging the equation (4) as the following expression:

$$t = -\frac{1}{\alpha_o + \alpha_1} \ln \frac{I_s}{I_o \beta (1 - R_o)^2 (1 - R_1)^2} = \frac{-1}{\alpha_o + \alpha_1} [\ln I_s - \ln I_o \beta - \ln (1 - R_o)^2 (1 - R_1)^2] \quad (5)$$

Therefore, by independently measuring the R_o , R_1 , and $I_o \beta$, and obtaining the absorption coefficients, the thickness of a-C:H coatings can be calculated based on I_s . Here, the absorption coefficient (α) of a-C:H can be obtained by

$$\alpha = \frac{1}{-t} \ln \frac{T}{(1 - R)^2} \quad (6)$$

which derives from equation (3) and t is measured by optical profilometer (Figure S1).

For comparison, the calculated thickness of a-C:H based on the Raman signal of carbon (I_G , G band at 1555 cm^{-1}) are also provided according to the previous studies [15,16]. The Raman intensity of carbon signal can be calculated by integrating contribution from each slice over thickness t (Figure 1c) by

$$I_G = I_{c\infty} (1 - R_o)(1 - R_2) [1 - \exp(-\alpha_o - \alpha_2) t] \quad (7)$$

which can be rewritten as

$$t = \frac{-1}{\alpha_o + \alpha_2} \ln \left[1 - \frac{I_G}{I_{c\infty}(1-R_o)(1-R_2)} \right] \quad (8)$$

where $I_{c\infty}$ is the intensity obtained at saturation for infinitely thick layer, R_o and α_o are the reflectivity and absorption coefficient of a-C:H for incident light (488 nm), and R_2 and α_2 are the reflectivity and absorption coefficient of a-C:H for incident light (528 nm for the G band of carbon signal). Since G peak arises from the stretching vibration of all sp^2 sites in both aromatic rings and C=C chains while D peak only derives from sp^2 sites in rings, G peak intensity (I_G) is employed to quantify the thickness of a-C:H coatings in this study [15].

3.2. Thickness Quantification of as-grown a-C:H Coatings

The a-C:H coatings with different thicknesses were deposited on both silicon wafers and glass plates in the same batches by PECVD method. For transmittance and reflectivity acquisitions, UV-vis-NIR spectroscopy was employed to characterize the samples with a-C:H deposited on glass plates, and the spectra in the wavelength region 400 to 600 nm were displayed in Figure 2a,b. With increasing the thickness of a-C:H coatings, a significant decrease of transmittance values was observed, while the reflectivity values fluctuated between 19 % and 25%. Table S1 summarized the optical parameters at wavelength of 488, 500 and 528 nm, which was used to calculate the coating thickness.

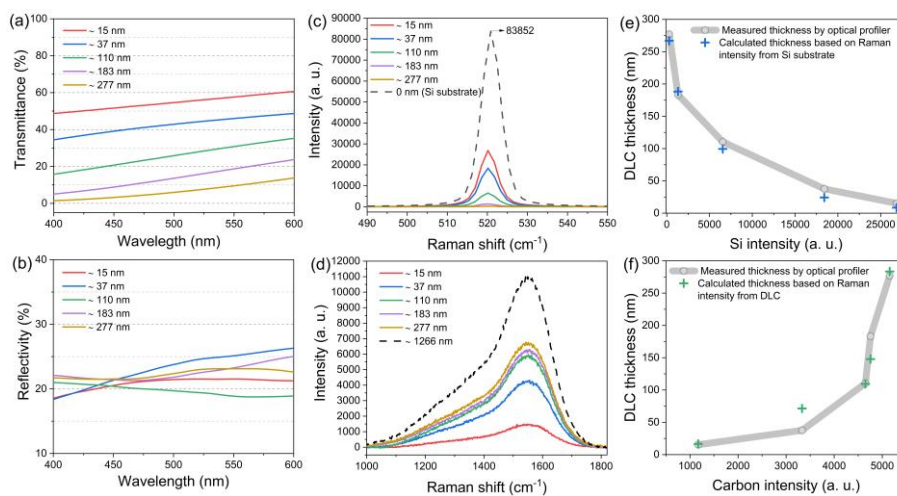


Figure 2. Transmittance spectra (a) and reflectivity spectra (b) of as-grown a-C:H films of different thickness deposited on glass substrate. Raman spectra of as-grown a-C:H films of different thickness

deposited on silicon wafers (c, silicon 1st band; d, carbon band). Comparison between the measured thickness of as-grown a-C:H films by optical profilometer and calculated thickness based on Raman intensity of silicon band (e) and G peak of carbon band (f).

Figure 2c,d displayed Raman spectra of silicon 1st band and carbon band of samples (a-C:H coatings of different thickness deposited on silicon wafers). The Raman intensity of silicon signal corresponds to the peak value of silicon 1st band, while that of carbon signal (G peak) could be obtained through Gaussian fitting. As shown in Figure S2, two Gaussian peaks fitting was used in the shape fitting of carbon band as it works better for hydrogenated amorphous carbon, especially for the condition with a photoluminescence background [22].

Once the optical parameters of a-C:H coatings were obtained (Table S1), the calculated thicknesses based on the Raman signals of silicon and carbon could be calculated according to equations (5) and (8), respectively. Figure 2e,f and Table S2 summarized the calculated thicknesses based on I_s (Raman intensity of silicon) and I_G (Raman intensity of carbon) and measured values by non-contact optical profilometer. The calculated thickness of a-C:H coatings showed good alignment with that of optical profilometer. It can be observed that the a-C:H thickness decreased logarithmically with increasing I_s in Figure 2e, which is in accordance with equation (5), while the opposite trend was observed in the result based on Raman intensity of carbon as shown in Figure 2f, which can be verified by equation (8).

3.3. Wear Measurement of a-C:H Coating from a Dry Friction Test

Tribological tests, with time ranging from 10 to 110 mins, were performed directly on the sample (a-C:H of 277 nm thickness on silicon wafer) at applied load of 1N (~ 550 MPa), velocity of 10mm/s, room temperature around 25 °C, and atmospheric environment. Figure S3 shows corresponding friction curves and optical images of middle areas of wear scars. To verify the accuracy and error tolerance capacity of the proposed method, a tribo-tested sample (90 mins) was thoroughly investigated in this section by combining Raman,

TEM, EELS and profilometers in order to reveal the influence of tribo-induced effects on the measurement accuracy.

As shown in Figure S4a, a line-scanning Raman spectroscopy was conducted across the wear track and the spectra of silicon and carbon signal were presented in Figure S4b,c respectively. Figure 3a gave the corresponding Raman intensity values of silicon bands and carbon G peaks and A_D/A_G ratios (area ratios of D peak and G peak). Then the coating thickness values across the wear scar could be obtained according to the equation (5) and (8). After subtracting the thickness value of as-grown a-C:H, the wear profile curves were given in Figure 3b. It could be observed that, at the edges of the wear scar, the wear profile deriving from the silicon signal compared well with that of carbon signal. However, as approaching to the centre region, the wear profile based on carbon signal displayed sharp depth rising, while that corresponding to silicon signal displayed a consistent downward trend.

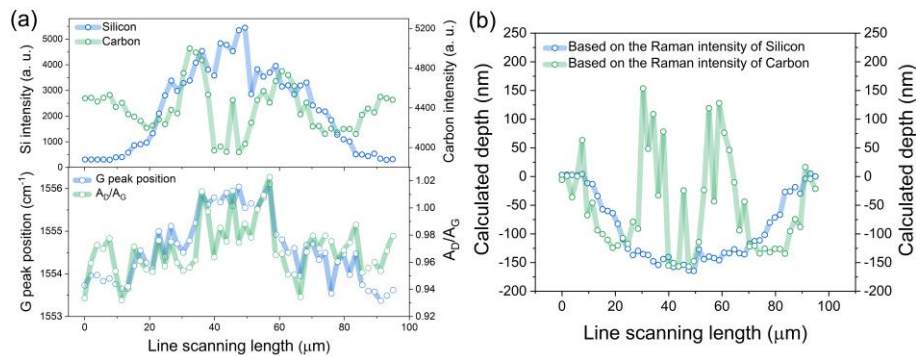


Figure 3. (a) Intensity of silicon bands, intensity and position of G peak of carbon bands, and area ratios of D peak and G peak (A_D/A_G). A_D/A_G increases obviously in the center region of wear track indicating the increase of sp^2 fraction. (b) Calculated wear profile curves based on the Raman intensity of silicon signal and carbon signal.

To validate these two methods, non-contact optical profilometer and contact profilometer were used to characterize the same sample as shown in Figure S5. It is well known that non-contact optical profilometer builds up 3D map by collecting array signals of light interference of reflected light (for example, the highest points on the surface will cause interference first). Due to its high sensitivity towards optical signal, the variation of optical properties (i.e., reflectivity) on the top surface, arising from tribo-induced

polishing effect [23-25], could affect the intensity of light signal and further results in coating thickness mismatch with the actual. As shown in Figure S5b,e, it was found that after depositing an iridium layer (~ 20 nm in Figure S6) the depth rising emerging in the wear profile disappeared. This was because the iridium layer could provide a top surface with consistent optical properties. Here, the contact profilometer was employed to verify the feature information of wear profile (e.g., depth rising) rather than the accuracy as its low resolution could result in obvious measurement errors. As shown in Figure S5c, the measured result of contact profilometer confirmed the absence of depth rising inside the wear scar. The depth rising appearing in the edge should be due to the low resolution of the measuring mode of contact profilometer considering the similar width (90 μm of contact profilometer vs 87 μm of non-contact optical profilometer). To further verify the results of optical profilometer, FIB with in-situ lift-out technique was used to fabricate lamellar specimens in three typical areas of wear scar for obtaining the actual coating thickness by combination of TEM characterization. More details are presented in S2 and Figure S7-10. Figure 4a-c includes the results of non-contact optical profilometer (with iridium layer), TEM (FIB), and our quantification method for comparison. It was confirmed once again that there was no depth rising region in the side area as shown in Figure 4b. Meanwhile, it is suggested that after depositing an iridium on the surface of tribo-tested sample, the optical profilometer could be used to provide accurate wear depth and this method will be employed as standard reference to verify the results based on Raman signal in this study.

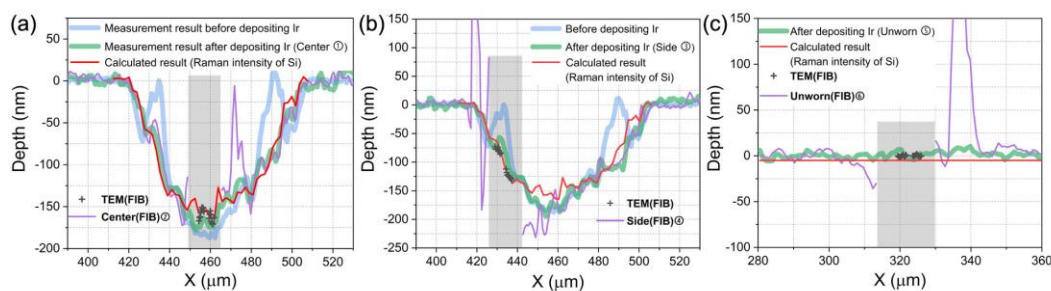


Figure 4. (a)-(c) Comparison of the wear profile curves obtained by different methods (90 mins tribo-test). Non-contact optical profilometer: wear profile curves before (blue line) and after depositing iridium layer (green line), and wear profile curves after FIB (purple line). Wear quantification method based on the Raman intensity of silicon signal (red line). Combination of FIB, SEM, and TEM measurements: actual thickness values (+) in the marked areas of (a) and (b). Grey areas are corresponding to targeted FIB areas.

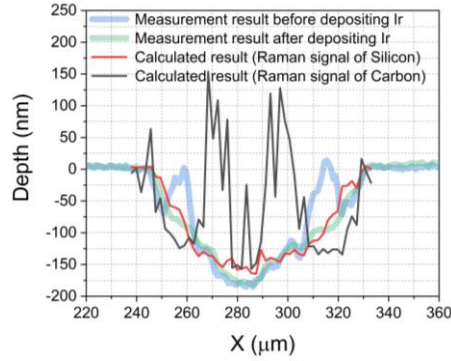


Figure 5. Comparison between calculated wear profile derived from Raman intensity of silicon and carbon bands and measured wear profile characterized by non-contact optical profilometer (before and after depositing iridium layer on top of a-C:H).

Figure 5 includes the results from optical profilometer, and the calculated results based on Raman signals of carbon and silicon for comparison. It could be observed that the wear profile curve deriving from Raman signal of silicon showed good alignment with that measured after depositing the iridium layer by optical profilometer, which demonstrated the accuracy of our coating thickness quantification method. While for the depth rising in the result based on Raman signal of carbon, it should derive from the tribo-induced enhancement of sp^2 phase (i.e., the increase and local clustering of sp^2 -C phase (rearrangement of bond structure to six-fold rings)), in view of the increase of A_D/A_G and up-shift of G peak position emerging in the regions of depth rising (Figure 3a) [17,26,27]. This is because Raman spectra of carbon of a-C:H are dominated by scattering of sp^2 phase due to its high polarizability. Slight enhancement of sp^2 phase, especially ordering or clustering, could result in remarkable increase of the Raman intensity [17], further leading to disagreement in the bonding transformation regions.

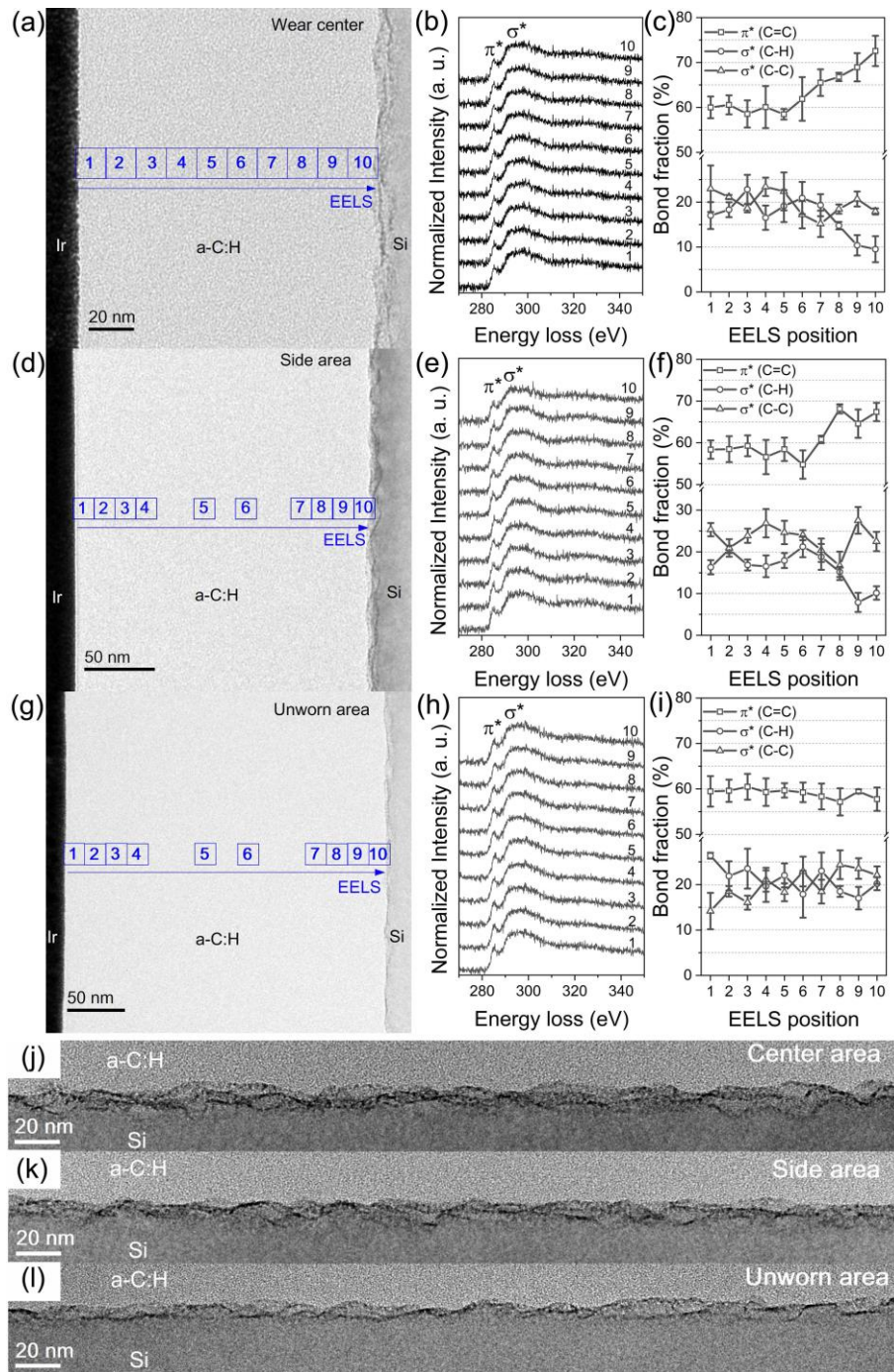


Figure 6. TEM images showing the cross-sectional morphology of FIB lamellar specimens from the center area (a), side area (d) and unworn area (g) as marked in Figure 5, evolution of C-K EELS (STEM) core-edge spectra recorded across the cross-sectional area from the wear center (b), side area (e) and unworn area (h) as marked in (a), (d) and (g) respectively, and evolution of the calculated EELS C-bonds fractions across the cross-sectional area from the wear center (c), side area (f) and unworn area (i) from the EELS C-K edges presented in (b), (e) and (h). *Error bars* denote s.d. of calculated bond fractions. TEM images of the cross-sectional morphology of the interface areas between a-C:H and Si wafer from center area (j), side area (k), and unworn area (l). The thickness of layer with nanovoid increase as it moves towards to wear center.

To explore the underlying mechanism of this kind of tribo-induced bonding transformation, the bonding structure of the above FIB specimens from three targeted areas were further examined by EELS. Figure 6 present the EELS spectra (STEM mode) of C-K core-edge collected point by point across the specimens. By fitting the C-K edges via two Gaussian peaks, more accurate bonding information can be obtained (Figure S11). Figure 6c,f,i display the evolution of the calculated bonds fractions in the C-K edges at targeted areas (Figure S7). The EELS result in Figure 6i confirmed the consistent bonding environment across the cross-sectional unworn area (as-grown a-C:H). The calculated sp^2 -C fraction was in the range of 55-60%, with residual fraction attributed to σ^* bonds (17-25% for C-H and 15-25% for C-C). While for the film in the wear center, it was divided into two sublayers according to the EELS result in Figure 6c: a top layer with bonding structure being similar to the case of unworn area and a bottom layer near the silicon substrate with remarkable increase of sp^2 phase (π^* (C=C), up to ~72%) and decrease of σ^* (C-H) fraction (down to ~10%). Similar trend could be found in the EELS result of side area (Figure 6f). It was hence reasonable to speculate that the bottom layer underwent a bonding transformation of sp^3 (C-H) to sp^2 (C=C).

This critical finding further raised an interesting and important question why bonding transformation was observed on the a-C:H/silicon interface rather than the top sliding interface. Based on the previous findings about the tribo-chemical reaction of a-C:H under different test environments [28-34], the absence of bonding transformation on the sliding interface was attributed to the combined actions of easy-oxidation of a-C:H and easy-shear capability of the oxidation product during friction process. Surface analysis of the oxide layer of a-C:H indicated that the oxidation resulted in the C-C or C-H bond dissociation and rearrangement of bond structure to disordered sp^2 phase, accompanied by the alteration of the mechanical properties which make oxide layer more prone to wear [28,29]. Especially under high oxygen pressure, the removal of transfer film (oxide layer)

was almost complete inside the wear scar, and loose wear debris could only be observed on the edge areas around the two ends of sliding direction [31,35], which was in accordance with our test results (Figure S12). Therefore, we could not observe structural or phase transformation on the top surface of a-C:H coating. On the other hand, TEM images in Figure 6j-l detected a sublayer with growing nano-porous structure formed on the bottom area of a-C:H coating. As displayed in Figure 6l, a porous layer with thickness up to ~10 nm was observed in the unworn area (as-grown a-C:H), which should result from the thermally activated release of hydrogen from the a-C:H coating during the high temperature deposition process [36,37]. Besides, it was interesting to note that the porous sublayer in the sliding contact areas became more prominent with the thickness increasing to ~20nm after the tribological test (Figure 6j,k). As indicated in the literature, hydrogen emission was detected during friction from PECVD a-C:H coating as the main product of tribo-chemical degradation [38] and could result in a relatively porous structure [39]. Meanwhile, the existence of the porous structure, especially more nanopores emerged in the wear center, triggered high stress concentration and further prompted the phase transformation during friction [18]. In addition, it should be pointed out that silicon is well known for its role in contributing to the formation of a porous microstructure (micro-void) in the $\text{Si}_{1-x}\text{C}_x\text{:H}$ alloys [40]. Therefore, it was suggested that this stress concentration due to structural evolution should played a pivotal role in the bonding transformation, where hydrogen atoms were cleaved from C-H on the local stress-concentrated points, leaving C atoms rehybridized into disordered sp^2 carbon bonds, as the activation energy barrier for C-H to C=C was significantly lower than that for C-C to C=C [41,42].

It is necessary to clarify the reason why the coating thickness method based on Raman signal of silicon could avoid the remarkable errors caused by the tribo-induced bonding transformation. As shown in Table S3, the average values of EELS bonds fractions across the test areas were summarized. It can be observed that the average value of sp^2 fraction

in the unworn area is $\sim 59\%$. In comparison, only a small increase of the sp^2 fraction appear in the side area and center area ($\sim 60\%$ for side area, $\sim 63\%$ for center area). Therefore, the tribo-induced bonding transformation should have slight effect on the optical properties of the whole coating and the final Raman intensity of silicon signal. Considering the noticeable enhancement effect of sp^2 phase on Raman intensity of carbon signal, the method based on the Raman signal of silicon is expected to provide more accurate value of a-C:H thickness in friction process.

3.4. Wear measurement in dry and oil-lubricated condition

3.4.1. Wear measurement in dry friction test

The aim of the coating thickness quantification method is developing a wear measurement system. Figure 7 shows the wear profile curves of different tribo-test time obtained by both optical profilometer and our quantification method. As discussed in section 3.3, through depositing an iridium layer on top of wear scar, an accurate wear profile by non-contact optical profilometer could be obtained. This method was employed here to verify the calculated wear results deriving from the Raman signal of silicon. Through comparison, our quantified results compared well with the measured results by optical profilometer in all tribo-tests. Specifically, our thickness quantification method could not only provide accurate values of maximum width and depth, but also detailed information about depth evolution along the wear profile, which was crucial to wear monitoring and service-life prediction of coatings. However, it was also noted that there existed bigger difference between these two methods when the maximum wear depth was lower than 20 nm (Figure 7a).

In addition, Figure 7i displays the evolution trend of wear scar, and it is observed that the maximum width and depth of wear scars increase linearly with test time. This could be used to monitor the wear and predict the service life of coatings. On the other hand, when using optical profilometer, there was remarkable difference between the results

before and after depositing iridium layer, which was significantly intensified by the tribo-induced polishing effect on some contact areas, especially in the long term test (60-110 mins, Figure 7f-h).

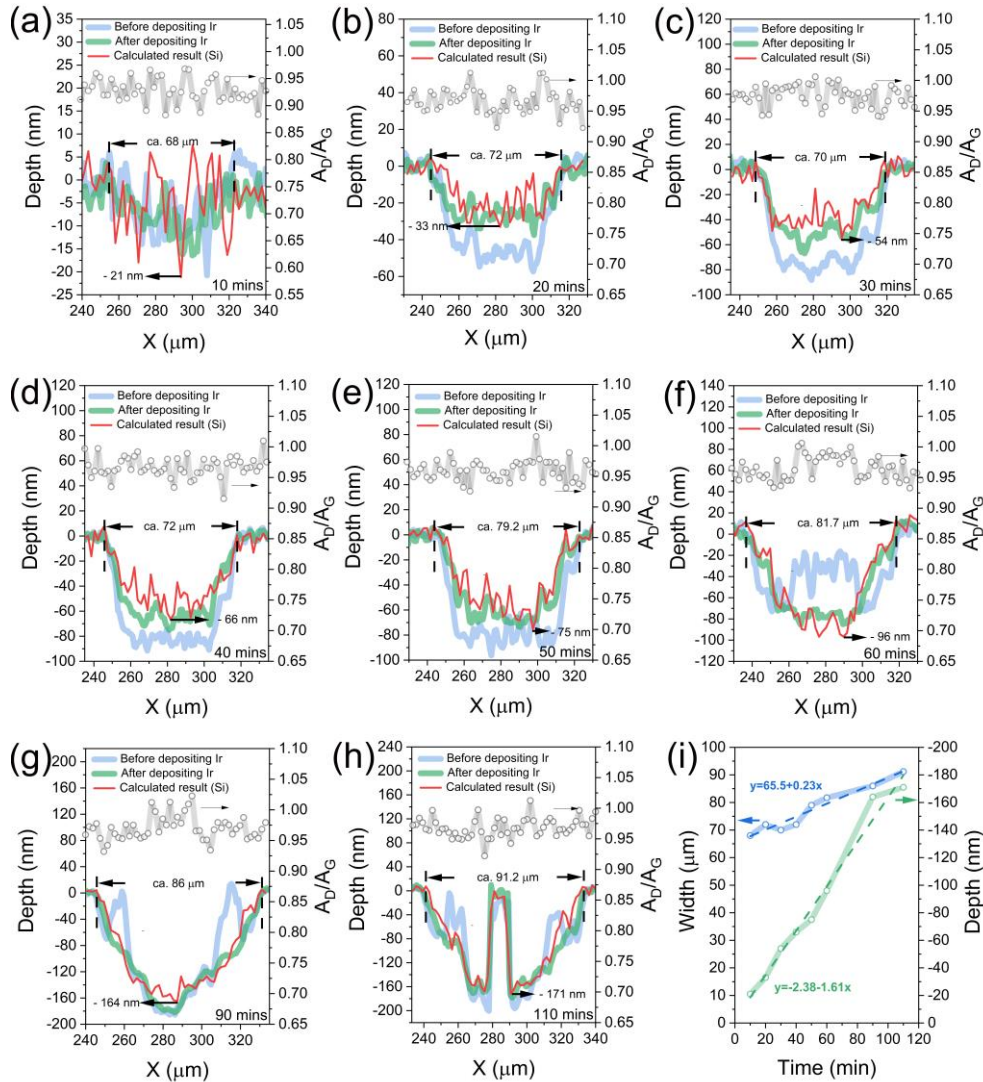


Figure 7. (a)-(h) Comparison of the wear profile curves obtained by different methods (dry friction with test time range 10-110 mins). Non-contact optical profilometer: wear profile curves before (blue line) and after depositing iridium layer (green line). Wear quantification method based on the Raman intensity of silicon signal (red line). The A_D/A_G ratios across the wear scars (grey line). (i) Evolution of width and depth of wear scars with test time.

3.4.2. Wear measurement in oil-lubricated test

The most critical finding in this study is the application of our method to quantify the coating thickness in oil-lubricated sliding conditions. Here, PAO base oil was used as lubricant in tribo-test (Figure S13) and the tested samples were transferred directly to Raman spectroscopy for characterization without removing PAO. To verify the quantified

results, the tested samples were also characterized by optical profilometer after removing the oil film with heptane and depositing iridium layers, and the results were employed as standard references.

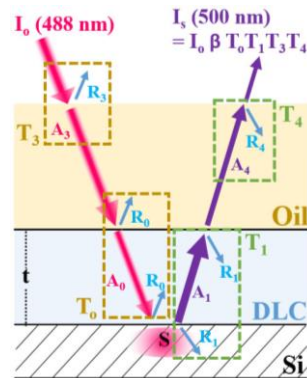


Figure 8. Schematic illustration of the coating thickness quantification methods under oil-lubricated condition.

Figure 8 illustrates the principle of coating thickness quantification under oil-lubricated condition. Based on the assumption that the oil film with roughly same thickness could be formed on the top of coating under stable friction process and small thickness difference of oil film could not result in significant error of quantified results due to the high transmittance of PAO, the Raman intensity of silicon signal could be obtained by

$$I_s = I_o \beta T_o T_1 T_3 T_4 \quad (9)$$

where β is light scattering rate, $I_o \beta$ is Raman intensity of silicon 1st band of silicon substrate, T_o and T_1 are transmittance values of incident light and scattered light in a-C:H, and T_3 and T_4 are transmittance values of incident light and scattered light in oil film.

Then, the coating thickness could be given by

$$t = \frac{-1}{\alpha_o + \alpha_1} [\ln I_s - \ln I_o \beta - \ln T_3 T_4 - \ln(1 - R_o)^2 (1 - R_1)^2] \quad (10)$$

which could be rewritten as

$$t - \frac{\ln T_3 T_4}{\alpha_o + \alpha_1} = \frac{-1}{\alpha_o + \alpha_1} [\ln I_s - \ln I_o \beta - \ln(1 - R_o)^2 (1 - R_1)^2] \quad (11)$$

where the effect of oil film in the form of $\frac{\ln T_3 T_4}{\alpha_o + \alpha_1}$ will result in the lowering of quantified thickness than the actual value. With knowing all parameters in the right of equation (11)

as stated in section 3.3, we could obtain the value of $t - \frac{\ln T_3 T_4}{\alpha_o + \alpha_1}$. After subtracting the thickness of as-grown a-C:H, the wear profile curves were obtained and displayed in Figure 9a-d (black lines). Clearly, the initial calculated results were far below the measured result by optical profilometer. Since T_3 and T_4 were regarded as constants based on the assumption above, $\frac{\ln T_3 T_4}{\alpha_o + \alpha_1}$ could be considered as a constant. It was therefore suggested the values of $t - \frac{\ln T_3 T_4}{\alpha_o + \alpha_1}$ taken point by point across the wear scar could reflect the actual variation trend of wear depth. When the value obtained on the edge (unworn area) was set as reference (for example, it is -35nm in Figure 9a (black line)), the expected wear profile was obtained by shifting up the reference value (red line in Figure 9). As displayed in Figure 9a-d, the revised wear profile curves compared well with that of optical profilometer (with iridium layers) in all tested samples. Figure 9e shows the evolution trend of wear width and depth with test time. Compared with the results under dry condition, the wear condition was significantly improved with the maximum width and depth reduction of ~25% and ~85% respectively.

It should be also pointed out that, when the initial quantified thickness (without tribotest) is set as reference, the difference between thickness obtained in the friction process and the reference value is just the wear depth and only depend on I_s according to the equation (5) and (10), as all the parameters except I_s could be regarded as constant for the same a-C:H sample. Furthermore, in view of the small wear depth under oil-lubricated condition, the sample of dry friction (110 mins) with larger wear depth (Figure 7h) was covered with PAO and used for verifying the quantification method under severe wear condition. As displayed in Figure 9f, it was confirmed that our method could provide accurate depth values under large wear depth. On the other hand, more prominent tribo-induced polishing effect happened under oil-lubricated condition (blues lines in Figure 9a-d). Compared with the results of dry friction (Figure 7), the polishing effect under oil-

lubricated condition appeared in the earlier stage (30 mins), due to the role of liquid in accelerating the polishing process.

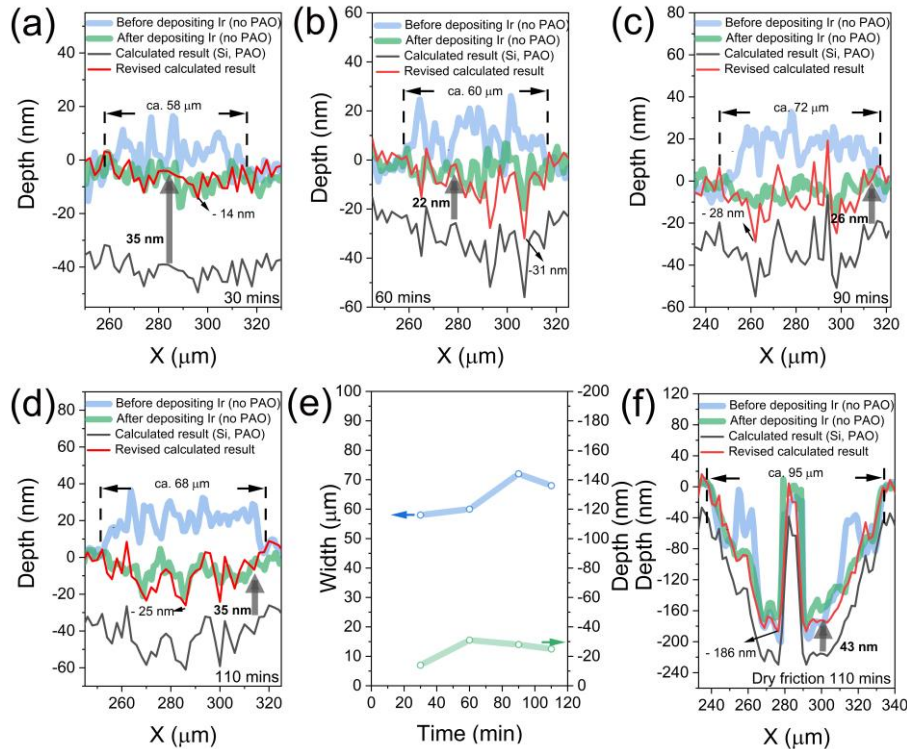


Figure 9. (a)-(d) Comparison of the wear profile curves obtained by different methods (oil-lubricated condition, PAO; test time 30-110 mins). Non-contact optical profilometer: wear profile curves before (blue line) and after depositing iridium layer (green line). Wear quantification method based on the Raman intensity of silicon signal (black and red lines). (e) Evolution of width and depth of wear scars with test time. (f) Comparison of the wear profile curves obtained by different methods. Here, we drop PAO on top of the tested sample under dry friction with test time of 110 mins as shown in Figure 7(h). Non-contact optical profilometer: wear profile curves before (blue line) and after depositing iridium layer (green line). Wear quantification method based on the Raman intensity of silicon signal with oil on top (black and red lines).

4. Conclusion

In this work, development and validation of a coating thickness quantification method was reported. This method was based on two functional layers: the top a-C:H served as light attenuating and anti-wear layer while the silicon substrate was employed as Raman-sensing layer. Since the Raman intensity of silicon signal varied as a function of a-C:H thickness, wear monitoring of a-C:H could be realized during the friction process, giving the opportunity for in-situ wear measurement. Compared with the results deriving from profilometer and Raman signal of carbon, coating thickness quantification method based

on the Raman signal of silicon provided more accurate wear profile in the long term tribo-tests. The remarkable errors of non-contact optical profilometer was attributed to the tribo-induced variation of optical properties on the top surface of a-C:H film, while the obvious errors of the approach based on Raman signal of carbon was due to tribo-induced bonding transformation of sp^3 (C-H) to sp^2 (C=C) in the bonding transformation regions, resulting in noticeable enhancement effect of sp^2 C-phase towards Raman intensity of carbon signal. More importantly, by introducing additional attenuating-layer of oil film into calculation process, this method enabled the possibility of monitoring coating wear under oil-lubricated condition. The developed coating thickness quantification approach, based on the system of target coating/Raman sensing layer, has the potential of quantifying the wear condition of diverse target coatings and may open a new pathway for (a) design and development of real-time wear monitoring and life prediction techniques for critical mechanical components and (b) design of novel and robust coating and lubricant systems.

Acknowledgements

The authors thank the helpful assistance for FIB and TEM tests by Mr. John Harrington, Mrs. Zebeada Aslam, and Mr. Stuart Micklethwaite from Leeds Electron Microscopy and Spectroscopy Centre (LEMAS), University of Leeds. The authors are grateful for facility access support by the Engineering and Physical Sciences Research Council (EPSRC, Grant no. EP/R02524X/1) in the UK.

References

- [1] K. Holmberg, A. Matthews, Coatings tribology-properties, mechanisms, techniques and applications in surface engineering, Elsevier, 2009.
- [2] X. Yang, W. Li, S. Yu, Y. Xu, K. Hu, Y. Zhao, Electrochemical characterization and microstructure of cold sprayed AA5083/Al₂O₃ composite coatings, *J. Mater. Sci. Technol.* 59 (2020) 117-128.
- [3] C. Guo, F. Zhou, M. Chen, J. Wang, S. Zhu, F. Wang, *J. Mater. Sci. Technol.* 70 (2021) 1-11.

- [4] I. El-Thalji, E. Jantunen, *Mech. Syst. Signal Process.* 60-61 (2015) 252-272.
- [5] G.Y. Lee, M. Kim, Y.J. Quan, M.S. Kim, T.J. Y. Kim, H.S. Yoon, S. Min, D.H. Kim, J.W. Mun, J.W. Oh, I.G. Choi, C.S. Kim, W.S. Chu, J. Yang, B. Bhandari, C.M. Lee, J.B. Ihn, S.H. Ahn, *J. Mech. Sci. Technol.* 32 (2018) 987-1009.
- [6] C. Scheffer, H. Kratz, P. Heyns, F. Klocke, *Int. J. Mach. Tool. Manuf.* 43 (2003) 973-985.
- [7] H. Shao, H.L. Wang, X.M. Zhao, *Int. J. Mach. Tool. Manuf.* 44 (2004) 1503-1509.
- [8] M. Nouri, B.K. Fussell, B.L. Ziniti, E. Linder, *Int. J. Mach. Tool. Manuf.* 89 (2015) 1-13.
- [9] Y. Zhou, X. Wei, *Int. J. Adv. Manuf. Technol.* 96 (2018) 2509-2523.
- [10] L. Dong-Hyeok, C. Nahm-Gyoo, *Meas. Sci. Technol.* 23 (2012) 105601.
- [11] C.Y. Poon, B. Bhushan, *Wear* 190 (1995) 76-88.
- [12] B. Bhushan, B.K. Gupta, *Handbook of tribology: materials, coatings, and surface treatments*, McGraw-Hill, 1991.
- [13] C. Muratore, D.R. Clarke, J.G. Jones, A.A. Voevodin, *Wear* 265 (2008) 913-920.
- [14] L. Fang, A. Yin, S. Zhu, J. Ding, L. Chen, D. Zhang, Z. Pu, T. Liu, *J. Alloys Compd.* 727 (2017) 735-743.
- [15] T.W. Scharf, I.L. Singer, *Thin Solid Films* 440 (2003) 138-144.
- [16] T.W. Scharf, I.L. Singer, *Tribol. Lett.* 14 (2003) 3-8.
- [17] J. Robertson, *Mater. Sci. Eng. R37* (2002) 129-281.
- [18] X. Chen, C. Zhang, T. Kato, X.A. Yang, S. Wu, R. Wang, M. Nosaka, J.B. Luo, *Nat. Commun.* 8 (2017) 1675.
- [19] X. Zhang, R. Schneider, E. Müller, D. Gerthsen, *Carbon*. 102 (2016) 198-207.
- [20] P.J. Larkin, *Infrared and Raman Spectroscopy; Principles and Spectral Interpretation*, Elsevier, 2011.
- [21] P.K. Chu, L. Li, *Mater. Chem. Phys.* 96 (2006) 253-277.
- [22] C. Casiraghi, A.C. Ferrari, J. Robertson, *Phys. Rev. B* 72 (2005) 85401-85414.
- [23] H. Liang, F. Kaufman, R. Sevilla, S. Anjur, *Wear* 211 (1997) 271-279.
- [24] Y.W. Zhao, L. Chang, *Wear* 252 (2002) 220-226.
- [25] X. Lu, K. Yao, J. Ouyang, Y. Tian, *Wear* 326 (2015) 68-73.
- [26] P. Manimunda, A. Al-Azizi, S.H. Kim, R. Chromik, *ACS Appl. Mater. Interfaces* 9 (2017) 16704-16714.
- [27] J. Xu, X. Chen, P. Grutzmacher, A. Rosenkranz, J. Li, J. Jin, C. Zhang, J. Luo, *ACS Appl. Mater. Interfaces* 11 (2019) 25535-25546.

- [28] D.Y. Wang, C.L. Chang, W.Y. Ho, *Surf. Coat. Technol.* 120 (1999) 138-144.
- [29] A. Alazizi, A. Draskovics, G. Ramirez, A. Erdemir, S.H. Kim, *Langmuir* 32 (2016) 1996-2004.
- [30] M. Marino, *Langmuir* 27 (2011) 12702-12708.
- [31] J. Fontaine, T. Le Mogne, J.L. Loubet, M. Belin, *Thin Solid Films* 482 (2005) 99-108.
- [32] M. Yang, M.J. Marino, V.J. Bojan, O.L. Eryilmaz, A. Erdemir, S.H. Kim, *Appl. Surf. Sci.* 257 (2011) 7633-7638.
- [33] H.I. Kim, J.R. Lince, O.L. Eryilmaz, A. Erdemir, *Tribol. Lett.* 21 (2006) 53-58.
- [34] J. Shi, Z.B. Gong, Y.F. Wang, K.X. Gao, J.Y. Zhang, *Appl. Surf. Sci.* 422 (2017) 147-154.
- [35] J. Shi, Z. Gong, C. Wang, B. Zhang, J. Zhang, *Diamond Relat. Mater.* 77 (2017) 84-91.
- [36] M. Malhotra, S. Kumar, *Diamond Relat. Mater.* 6 (1997) 1830-1835.
- [37] T. Zecho, B.D. Brandner, J. Biener, J. Kupperts, *J. Phys. Chem. B* 105 (2001) 6194-6201.
- [38] A. Rusanov, R. Nevshupa, J. Fontaine, J.M. Martin, T.L. Mogne, V. Elinson, A. Lyamin, E. Roman, *Carbon* 81 (2015) 788-799.
- [39] A. Erdemir, C. Donnet, *J. Phys. D Appl. Phys.* 39 (2006) R311-R327.
- [40] D.L. Williamson, A.H. Mahan, B.P. Nelson, R.S. Crandall, *Appl. Phys. Lett.* 55 (1989) 783-785.
- [41] A. Sattler, G. Parkin, *Nature* 463 (2010) 523-526.
- [42] S. Soltanahmadi, T. Charpentier, I. Nedelcu, V. Khetan, A. Morina, H.M. Freeman, A.P. Brown, R. Brydson, M.C.P. Eijk, A. Neville, *ACS Appl. Mater. Interfaces* 11 (2019) 41676-41687.